Semiconductor Microcavity Lasers

Paul L. Gourley, J. R. Wendt, G. A. Vawter, M. E. Warren, T. M. Brennan, and B. E. Hammons

Sandia National Laboratories
Albuquerque, NM 87185

ABSTRACT

New kinds of semiconductor microcavity lasers are being created by modern semiconductor technologies like molecular beam epitaxy and electron beam lithography. These new microcavities exploit 3-dimensional architectures possible with epitaxial layering and surface patterning. The physical properties of these microcavities are intimately related to the geometry imposed on the semiconductor materials. Among these microcavities are surface-emitting structures which have many useful properties for commercial purposes. This paper reviews the basic physics of these microstructured lasers.

1. INTRODUCTION

The semiconductor laser was first demonstrated in 1962 and has undergone several stages of development to the present. Early versions were simple p-n junction devices in bulk GaAs that were neither efficient nor commercially viable. They did, however, demonstrate the remarkable features of high compactness and coherent light emission. In the 70's the use of heterostructures, epitaxially layered materials with two different bandgaps, made a dramatic improvement in the efficiency. The heterostructures allowed the carriers and photons to be simultaneously confined to maximize their overlap of their spatial distributions.

In the 80's refinement of the heterojunctions and use of strained layers increased the efficiency and lengthed the laser lifetime. High power linear arrays were demonstrated. Nearly all of these lasers emitted in the near infrared and were edge-emitting, relying on an optical cavity formed by two cleaved or etched facets normal to junction. In the mid-80's a revolutionary vertical cavity laser was developed. This laser cavity was formed by epitaxial semiconductor multilayer mirrors. The cavity was short, but the mirror reflectivity was very high. These cavities emitted coherent light in the direction normal to the wafer surface.

The 90's have seen other revolutionary changes in both edge- and surface-emitting semiconductor lasers. Some of these have occurred for edge-emitting devices. The first blue/green edge-emitting semiconductor lasers were recently demonstrated with II-VI compound semiconductors. Recently, vertical cavity lasers have been operated as large phase-locked arrays. These arrays have been integrated with binary optical to control the divergence and pattern of the emitted light. More fundamental changes in the geometrical form of the semiconductor lasers are in progress.[1] Developing lasers exhibit an incredible variety of forms including multilayer sandwiches,[2,3] posts,[4] waffle gridirons,[5] thumbtacks,[6] swiss cheese,[7] concentric rings,[8] and honeycombs.[9] Other exotic structural forms are still being conceived. A checkerboard geometry for a phase-compensated 2-dimensional surface-emitting laser is shown in Fig. 1.

The new geometries rely on modern epitaxial growth and surface processing to create microstructured lasers. Techniques like molecular beam epitaxy and metal organic vapor phase epitaxy allow sequential layering of different materials with atomic precision. Thin layers of thickness ~100 Å are used to confine electron and holes. Thicker layers of thickness ~1000 Å are used to make mirrors or waveguides to confine photons. Surface patterning using photo, electron, or ion beam lithography in

This work was supported by the United States Department of Energy under Contract DE-AC04-94AL85000.

conjunction with etching techniques are used to selectively remove layers across the wafer. Taken together, epitaxial layering and surface patterning allow the creation of 3-dimensional laser microstructures for efficient light generation and high brightness. This paper examines the influence of microstructure on properties of semiconductor lasers.

2. MICROCAVITIES FORMED BY EPITAXIAL LAYERING

A prime example of expitaxial microstructure is the vertical cavity surface-emitting laser which is built up with hundreds of epitaxial layers.[2,3] This remarkable structure comprises all of the components of a laser within a single crystal. It is a fundamental semiconductor optical structures which confines light much like a quantum well confines electrons. It can be used for light generation,[2,3] modulation[10] or switching.[11,12] As a laser, it can operate as a planar device, etched post, or 2-dimensional array. A cross section of such a laser is revealed in the micrograph of fig. 2. It comprises 3 basic sections: upper and lower mirrors surrounding a quantum well active region. The mirrors confine photons in the direction normal to the wafer plane. The active region is a source of spontaneous emission for starting the lasing process. It also provides gain to amplify the spontaneous emission. As shown in Fig. 3, these lasers feature efficient power output, circular beam cross section, low divergence, and narrow lasing linewidth.

2.1 Epitaxial mirrors and electrical injection

Each mirror section comprises periodic pairs of layers with high and low refractive index.[13-15] The refractive indices of GaAs and AlAs differ by only 22%, but 25 periodic pairs create a reflectance exceeding 99.9%. The individual layer thicknesses d correspond to a quarter wavelength of light, $d=\lambda/4n$ where λ is the wavelength and n the refractive index. For GaAs-like materials, λ=850 nm and n=3.5 so d= 630nm.

In an electrically injected laser, the mirror must not only reflect light but transport carriers across the layers and interfaces. A p-i-n structure is formed by doping the top mirror p-type, the bottom mirror n-type, and leaving the active region undoped. In a common injection scheme, protons are implanted in to the active region around a circular aperture ~10 μm in diameter.[16-18] Metal contacts are applied, the junction is forward biased, and carriers are driven through the mirrors and funnel through the active region.

The mirrors are heavily doped either n or p type to decrease the individual layer resistivity. However, barriers to interlayer transport arise from the large energy offsets (~500 meV) of the conduction and valence bands between layers. The problem is most severe for the holes in the p-type mirrors. Fortunately, it is possible to microstructure the interfaces to reduce the resistivity of the mirrors.[19] In this technique, the composition at the interface is piecewise graded to "round off" the abrupt step in the electrostatic potential. During operation of the laser, the energy bands are bent by the externally applied voltage bias. The discontinuities in the piecewise grade appear as small potential cusps (~100 meV) in the energy band profile. Holes are easily transported across these small potential cusps. Recent experiments have shown that the mirror resistivity can be lowered by more than an order of magnitude, from hundreds of ohms to tens of ohms for a 20 micron circle. This resistivity is still quite high compared to conventional edge-emitting laser resistance (few tenths of an ohm). Further improvements are still needed.

2.2 Epitaxially microstructured active region

The above example shows how the mirror electrical properties can be improved by artificial structure. The active region can benefit from artificial structure as well. Structuring the gain region includes placing the

quantum wells periodically (periodic gain), inserting strained layers, or controlling the length of the active region. Periodic gain and strained layers improve the efficiency of the lasing process. The length of the active region influences the temperature dependence of the lasing threshold current. It also controls the photon dynamics within the laser cavity.

The active region comprises quantum wells to confine carriers and produce gain. Detailed theoretical analyses of quantum well gain, including many-body effects and coulomb enhancement have been developed.[20,21] These theories provide much valuable insight into the lasing physics. Most theories apply to the ideal case of electrons, holes, and photons distributed uniformly in space. An outstanding problem is to examine the effects of nonuniform distributions in microstructured resonators. Another experimental problem is to accurately measure the gain spectrum to compare with theory.

To illustrate the effects of gain in microstructured lasers, we begin with a simple analytic approximation for the optical gain g_q in a quantum well,

$$g_q = \frac{4\pi^2 e^2 M^2 \mu}{ncm^2 \omega \hbar^2}\left[f_c(\omega'\mu/m_c) - f_v(\omega'\mu/m_v)\right] \qquad (1)$$

where n is the refractive index, e and m are the free electron charge and mass, M is a momentum matrix element, and μ is the reduced mass. The quantity $\hbar\omega'=\hbar\omega-E_g$ is the photon energy reduced by the semiconductor bandgap energy E_g. The f_i are the 2-dimensional Fermi distribution functions for the conduction (c) and valence (v) bands, respectively. The onset of gain occurs when $f_c=f_v$ at carrier density σ_{tr} where the material becomes transparent. A gain function is plotted in the top of Fig. 4 for a 2-dimensional carrier density $\sigma=1\text{x}10^{12}$ cm^{-2} at 300K. The width of this gain function is $\Delta\hbar\omega=\mu_c+\mu_v$ where the μ_i are the chemical potentials of the conduction and valence bands. The bandwidth of the gain in Fig. 4 is about 50 meV.

Many-body interactions of carriers in the quantum wells alter the gain function.[22] the energy bandgap E_o is renormalized and the energy position of the gain curve decreases. This energy shift is primarily a result of the exchange interaction. The exchange interaction $E_{ex}=-(4e^2/\pi\kappa)(2\pi\sigma)^{1/2}$ where κ is the static dielectric constant. The many-body effects on the gain spectrum play an important role in the laser's temperature characteristics as we shall discuss shortly. The total gain for mode m is a sum over the positions z_i of the quantum wells,

$$G = \sum\nolimits_i g_q^i \cos^2(k_m z_i + \phi) \qquad (2)$$

where k_m is the mode wavevector, and ϕ is the round-trip mirror phase. Periodic gain in the active region is created by growing quantum wells commensurately with the antinodes in the optical standing wave present in the lasing resonator.[23-25] In this case, the lasing wavelength is stabilized by phase-locking the wave to the gain regions. The gain material in the active region is more effectively utilized than it is in cavities without periodic gain (where quantum wells are placed incommensurately with the optical standing wave).[23] Experiments suggest that periodic gain can enhance the spontaneous emission process itself.[26,27]

2.3 Strained layers

The active region can even benefit from atomic microstructure, lattice strain. In strained layer epitaxy, very thin layers of lattice-mismatched materials are grown into the active region. The benefits of strained layers are enormous and have been extensively studied.[28] Biaxial compressive strain splits the degenerate heavy and light valence bands. The occupied hole band has a light mass in the wafer plane and better matches the light conduction band mass. This confers significant benefits to the lasing process.[29,30] The carrier density σ_{tr}

required for population inversion is reduced. The transparency density is shown in Fig. 5 as a function of the conduction to valence mass ratio. For GaAs this ratio is 0.16, giving $\sigma_{tr}=1.2\times10^{12}$ cm^{-2}. For InGaAs strained-layer lasers,[31,32] the ratio is 0.5 and σ_{tr} is reduced about 30%. The threshold current for lasing is reduced, heating effects are minimized, and the lifetime of the laser is extended.

The use of strained-layer quantum wells is ideally suited to periodic gain. Strained layers must be kept thinner than the critical layer thickness for the onset of dislocation formation. With periodic gain this condition can easily be met. The strained layers can have thicknesses the order of 100 Å and be placed about 1300 Å apart. This relatively large spacing between strained layers keeps the average strain to a very small value and avoids dislocation formation.

2.4 Microstructure and temperature characteristics

The temperature dependence of these lasers is influenced by the interplay of the longitudinal optical modes and the gain spectrum.[22,23] These modes occur at energies $\varepsilon_m=\hbar c(2\pi m-\phi_1-\phi_2)/2Ln$ when an integral number of half waves fit into the length L of the active region. Two longitudinal modes are shown in the wafer reflectance spectrum in Fig. 4. The spacing of the modes is $\Delta\varepsilon_m\approx(hc/2L)/(n+\varepsilon_m dn/d\varepsilon)$. Usually the active region is about 1 or 2 μm long. This ultrashort laser length provides longitudinal modes which are widely spaced by about 80 meV which is wider than the gain spectrum. Usually only one longitudinal mode is present within the spectral bandwidth ~150 meV of the mirrors. It is crucial to position the mode at the peak gain. If the mode occurs at higher energy than the gain peak, a larger carrier density and Fermi energy are required to fill the bands and broaden the gain spectrum to achieve lasing. If the mode occurs at lower energy than the gain peak, a larger carrier density will renormalize the bandgap and gain spectrum, via many-body exchange interaction, to achieve lasing. So, misalignment of mode and gain can be compensated but at the cost of higher carrier density and current for lasing threshold. The lowest threshold current will occur when the mode is aligned to the renormalized bandgap at lasing threshold.

These microlasers have unique temperature characteristics. The alignment of the mode and gain spectrum will change with temperature. The gain spectrum moves to lower energy directly with the temperature dependence of the bandgap or about 5 meV/K. The modes move more slowly to lower energy by about 1 meV/K via the temperature dependence of the refractive index of the active region. These changes are shown in Fig. 6a. At low and high temperature, the gain and mode will misalign. At some intermediate temperature the gain and mode will align exactly. At this temperature the threshold current will be minimized. Experimental confirmation of this behavior is shown in Fig. 6b. The temperature of the minimum can be designed for slightly above ambient. As the laser heats during operation, the threshold current will decrease and the laser efficiency and lifetime will increase.

It is useful to compare these temperature characteristics to those in conventional edge-emitting lasers. In those lasers, the cavities are very long (several hundred micrometers) resulting in many closely spaced modes. Consequently, there are always many modes aligned with the gain spectrum. The lasing energy occurs at the peak of the gain spectrum and moves with the temperature dependence of the bandgap. The magnitude of the gain decreases monotonically with temperature. As a result, the lasing threshold current increases monotonically with temperature. Unlike the microlasers, there is no temperature minimum.

2.5 Microstructure and cavity dynamics

Microstructure has a profound effect on the temperature characteristics of semiconductor lasers. As well, it influences the carrier-photon dynamics within the optical cavity. This can be illustrated with a simple model. Consider a single quantum well inside a vertical cavity containing several optical modes. The modes

will have various spatial distributions depending on the cavity geometry. some of the modes will have good spatial overlap with the quantum well gain region. Others will not. This overlap will influence both the spontaneous and stimulated emission of photons into the modes. the 2-dimensional photon density π_m in a given mode is coupled to the 2-dimensional carrier density σ by the following rate equations,[34,35]

$$\dot{\sigma} = J - \gamma_e \sigma - \sum_m G_m \pi_m - \sigma \sum_m \gamma_m \tag{3a}$$

$$\dot{\pi}_m = (G_m - \gamma_c)\pi_m + \gamma_m \sigma \tag{3b}$$

where J is the injection rate of electron-hole pairs into the quantum well, γ_e is the nonradiative recombination rate. G_m is the gain, π_m is the photon density, and γ_m is the spontaneous emission rate into the mth mode. The quantity γ_{cm} is the cavity loss rate which includes mirror loss and cavity dissipation. This loss rate can be dominated by the mirror loss $\gamma_{mir}=(c/2Ln)\ln(1/R_1R_2)$, where c is the speed of light, n is the refractive index, and the R's are the mirror reflectance values at the mode wavelength.

Steady state solutions to eqns 3 can be classified by two microstructural parameters, the mirror loss $\delta=1-R_1R_2$ and the number of quantum wells N. A lasing phase diagram has been constructed in the δ vs N plane.[35] Stable lasing with optimum output efficiency occurs for microcavities with $\delta \approx 0.01N$. For a single quantum well, this implies that the mirror reflectance product must be 0.99.

The dynamics of the light output are governed by G and γ_c.[36,37] The risetime $\tau_r \approx 1/(G-\gamma_c)$ and the falltime $\tau_f \approx 1/\gamma_c$. Thus the laser risetime can be shortened by injecting higher current pulses and increasing G. The falltime is always fixed by the cavity loss rate. The falltime represents the time it will take for the photon intensity in the cavity to decay to 1/e of its steady state value after lasing has ceased. Lengthening the cavity or increasing the mirror reflectivity will increase the cavity lifetime. For a 2 μm long cavity with mirror loss $\delta=1-R_1R_2=0.01$, the cavity lifetime is 5 ps. Thus, the laser's intrinsic frequency response is up to 70 GHz. In practice, however, parasitic capacitance limits the response to below 10 GHz.[38,39]

The cavity lifetime can be decreased by selectively etching away pairs of quarter-wave layers. If many pairs are removed, the lasing action can be quenched entirely. This presents a novel way of creating large 2-dimensional arrays of lasing elements as shown in Fig. 7. By etching surface channels of ~1 μm width and 5 μm period in 2 orthogonal directions, square arrays resembling waffle gridirons have been formed.[5,40] When these array are operated as lasers by photopumping, the near field appears as shown in Fig. 8. Below the lasing threshold, the spontaneous intensity of emitted photons is high in the etched channels and much lower in the unetched regions. This demonstrates the decrease in photon confinement as the mirror periods are removed. Above the lasing threshold, the unetched regions support lasing and the emission becomes much more intense than that from the etched channels. The array operates in a phase-locked condition where every lasing element is precisely in phase with all the others. Other phase-locked arrays have been produced by metal grids deposited on the wafer surface.[41]

3. MICROSTRUCTURE BY SURFACE PATTERNING

At this point, the discussion has turned from microstructuring by epitaxial layering to microstructuring by surface pattering. The former is used primarily to enhance the efficiency of the lasing process. The latter is used primarily for shaping and directing the beam of light emitted from the wafer. Surface patterned arrays also provide a unique opportunity to study the interaction of light with 2-dimensional periodic materials.

3.1 2-dimensional arrays

Surface patterned vertical cavity wafers are useful for studying optical modes in a 2-dimensional array.[5,40-42] The optical mode in the array will determine the angular distribution of light observed far from the array surface (far field). The far field patterns observed experimentally reveal four bright spots.[5] The spots are placed symmetrically 5 degrees away from the optical axis into each of the four quadrants of the far field as shown in Fig. 9 (upper left photo). The width of the spots is about 2 degrees, slightly broader than predictions $\theta \approx \lambda/D$ by diffraction theory where D is the diameter of the array. The surface patterned array has a beam with much lower divergence and higher brightness than a single element of the array.

Despite the advantages of narrower divergence and higher brightness, the beam intensity is off the optical axis (normal to wafer surface). Most applications require a single beam on the optic axis. The off axis beam is due to the array mode which corresponds to each element being 180 degrees out of phase with its neighbors. This antisymmetric mode dominates the lasing process. The mode amplitude has a zero crossing between elements, consistent with the quenching of lasing in the channels mentioned earlier. Attempts have been made to produce a symmetric mode with on-axis intenstiy, but with little success.

A more successful approach is to let the array lase in its preferred antisymmetric mode and then use epitaxial binary optics to adjust the phase in the near field.[43] In this case, an extra phase correction layer is grown above the top mirror. After growth, the layer is selectively removed above every other lasing element. This leaves a checkerboard pattern etched into the phase correction layer (shown in Fig. 1). In the squares with remaining material, the phase of the outgoing wave is retarded by 180 degrees with respect to the squares without the material. The phase front of the wave is now compensated across the entire array surface, as if the array was operating in a symmetric mode. The far field pattern comprises a bright lobe on the optic axis as desired. There are also secondary lobes off the optic axis, but these are weaker.

3.2 Photonic lattices

The above example shows how surface patterning of an extra epitaxial layer can be used to produce a phase transformation in a outgoing wave. A phase adjustment in the near field produces a dramatic change in the far field. The near field and far field are Fourier transform pairs. Study of the far field can provide valuable information about the optical modes in the array. These arrays are form of a generalized periodic optical structure called a photonic lattice.[44] Optical Bloch waves in the lattice are analogous to electron Bloch wavefunctions in a crystalline solid.[45-47] Within each unit cell of the lattice there exists a local optical symmetry. An additional translational symmetry exists for the array of unit cells. The local and translational symmetry combine to form an optical Bloch wave. The amplitude of this wave for a given polarization may be written

$$E(\mathbf{r}) = \sum_{\mathbf{k}_{B,\alpha}} e^{i\mathbf{k}_B \cdot \mathbf{r}} \sum_{n,\alpha} E_\alpha(\mathbf{r} - \mathbf{R}_n) \tag{4}$$

where $\mathbf{k}_B$ is a Bloch wavevector, $\mathbf{R}_n$ is a lattice vecor, and E_α is the unit cell wavefunction. For a square cell, the E_α are similar to the TEM_{mn} modes of a rectangular waveguide. The far field emission pattern is the 2-dimensional Fourier Transform of Eqn (4) and is given by

$$\xi_0(\mathbf{k}_S) = \sum_{\mathbf{k}_{B,\alpha}} \xi_\alpha(\mathbf{k}_S - \mathbf{k}_B) \sum_\ell \delta_{\mathbf{k}_B - \mathbf{k}_S - \mathbf{G}_\ell} \tag{5}$$

where $\mathbf{k}_s$ is the scattering wavevector, ξ is the Fourier transform of the unit cell mode and Kronecker delta function restricts the scattered wavevector to $\mathbf{k}_s = \mathbf{k}_B - \mathbf{G}_l$. Thus, for each wave $\mathbf{k}_B$ there will be a set of emitted (scattered) wavevectors $\{\mathbf{k}_s^l\}$ corresponding to a complete set of reciprocal lattice vectors. Locally, about each $\mathbf{k}_B$ the field amplitude will be distributed as the Fourier transform ξ. Since the cell size is about a, the angular spread of the envelope function ξ is about λ/a.

Wide angle far field patterns emitted from a 5 μm period lattice have been measured.[44] They show four dominant lobes and weaker diffraction lobes at wider angles. The weaker lobes are actually doublets. The presence of these doublets suggests that photons are partially confined in the wafer plane. This pattern can be used to map the Bloch states of the lattice.[44]

3.3 Photonic bandgap materials

The use of optical feedback in the wafer plane can be more fully utilized with a photonic lattice with period corresponding to half an optical wavelength. These structures have been proposed by Yablonovitch[48] and studied theoretically.[49] 3-dimensional structures for use at microwave frequencies have been demonstrated. Structures for optical frequencies have proven difficult to fabricate because of the small dimensions. 2-dimensional lattices which have a complete in-plane photonic bandgap have recently been proposed by Meade et al.[50] and Villeneuve and Piche.[51] Honeycomb lattices, triangular lattices of air holes, have a complete gap for both transverse electric and transverse magnetic polarizations as illustrated in Fig. 10. The maximum bandgap occurs in structures with ~85% air volume fraction.

Honeycomb nanostructures fabricated in compound semiconductors using elecron beam lithography and reactive ion beam etching are shown in Fig. 11. The honeycomb corresponds toa 2-dimensional second order Bragg reflector in the plane for optical wavlengths near 800 nm. This includes wavelengths for the spontaneous emission from GaAs quantum wells. These lattices are of interest for as active materials for semiconductor lasers or as passive materials for waveguides. Initial optical characterization of these lattices reveal that light normal to the plane can be resonantly coupled into the lattice near the Bragg condition.[52] Under these conditions the propagation of light can be studied. A photomicrograph of light propagated and scattered out of the lattice is shown in Fig. 12.

3.4 Other 3-dimensional microstructures

The use of 2-dimensional photonic lattices and mirrors is one approach to 3-dimensional confinement of light. Other approaches to confine light are also being investigated.[1] These include vertical cavity posts, hemispherical cavities, whispering gallery disks, and others. The object is to make small microcavities to localize a few modes from the surrounding free space modes. The cavity modifies the spontaneous emission rate. As well, it modifies the fraction β of spontaneous emission which is coupled into the lasing mode. As β approaches 1, the threshold current for lasing decreases, the lasing linewidth narrows, and the laser intensity fluctuations decrease.[53]

An approximation for the spontaneous emission coefficient at wavelength λ is

$$\beta \approx \frac{(\lambda/2n)^3}{V}\frac{\lambda}{\Delta\lambda_{sp}} \tag{6}$$

where $(\lambda/2n)^3$ is the optical volume per mode, V is the total cavity volume, and $\Delta\lambda_{sp}$ is the linewidth of the spontaneous emission spectrum. Large area vertical cavity surface-emitting lasers have $\beta \approx 0.01$. Posts etched into these laser wafers have $\beta \approx 0.1$. Even higher values $\beta \approx 0.2$ are attained with whispering gallery disks.[6] The values in photonic lattices and photonic bandgap materials are expected to approach 1, but have not yet been

demonstrated experimentally.

4. CONCLUDING REMARKS

An unprecendented capability to synthesis microstructures is changing the form of the semiconductor laser. The ability to confine single optical modes in subcicron laser laser resonators built within a single crystal is also changing the way we think about semiconductor lasers. It is possible to envision extremely high confinement resonators occupied by single photons. Low quantum occupation would allow entirely new kinds of photonic devices using minute power. These devices could become viable system components for transmitting, storing, and manipulating information. The conception, fabrication, and study of these device structures is creating new opportunities and exciting new challanges for scientists and engineers.

5. REFERENCES

1. Y. Yamamoto and R. E. Slusher, in *Physics Today*, **46**, 66 (1993).
2. K. Iga, F Koyama, and S. Kinoshita, J. Quantum Electron. **242**, 1845 (1988), and references therein.
3. P. L. Gourley and T. J. Drummond, Appl. Phys. Lett. **50** 1225 (1987).
4. J. L. Jewell, A. Scherer, S. L. McCall, A. C. Gossard, and J. H. English, **51**, 94 (1987).
5. P. L. Gourley, M. E. Warren, G. R. Hadley, G. A. Vawter, T. M. Brennan, and B. E. Hammons, Appl. Phys. Lett. **58**, 890 (1991).
6. S. L. McCall , A. F. J. Levi, R. E. Slusher, S. J. Pearton, R. A. Logan, Appl. Phys. Lett. **60**, 289 (1992).
7. E. Yablonovitch, T. J. Gmitter, and K.M. Leung, Phys. Rev. Lett. **67**, 2295 (1991).
8. T. Erdogan, O. King, G. W. Wicks, D. G. Hall, C. L. Dennis, and M. J. Rooks, Appl. Phys. Lett. **60**, 1773 (1992).
9. P. L. Gourley, J. R. Wendt, G. A. Vawter, T. M. Brennan, and B. E. Hammons, Appl. Phys. Lett., accepted for publication.
10. G. W. Yoffe, D. G. Schlom, and J. S. Harris, Jr., Appl. Phys. Lett. **51**, 1876 (1987).
11. O. Sahlen, U. Olin, E. Masseboeuf, G. Landgren, and M. Rask, Appl. Phys. Lett. **50**, 1559 (1987).
12. J. L. Jewell, A. Scherer, S. L. McCall, A. C. Gossard, and J. H. English, Appl. Phys. Lett. **51**, 94 (1987).
13. J. P. Van der Ziel and M. Illegems, Appl. Opt. **14**, 2627 (1975), **15**, 1256 (1976).
14. M. Ogura, T. Hata, N. J. Kawai, and T. Yao, Japan. J. Appl. Phys., **22**, L112 (1983).
15. See the review and references therein, by P. L. Gourley, R. M. Biefeld, T. J. Drummond, and T. E. Zipperian, in *Advances in Semiconductors and Semiconductor Structures*, SPIE vol. 792, 178 (1987). P. L. Gourley, Superlattices and Microstructures **1**, 227 (1985).
16. J. L. Jewell, A. Scherer, S. L. McCall, Y. H. Lee, S. Walker, J. P. Harbison, and L. T. Florez, Electron. Lett. **25** 1123 (1989). Y. H. Lee, J. L. Jewell, A. Scherer, S. L. McCall, J
17. Y. H. Lee, B. Tell, K. Brown-Goebeler, J. L. Jewell, and J. V. Hove, Electron. Lett. **26**, 711 (1990).
18. Other injection schemes cover the top mirror with metal and emit through the substrate, R. S. Geels, S. W. Corzine, J. W. Scott, D. B. Young, and L. A. Coldren, Photon. Tech. Lett. **2**, 234 (1990).
19. K. L. Lear, S. A. Chalmers, K. P. Killeen, and J. Zolper, paper CTuD2, Conf. on Lasers and Electro-Optics, May 2-7, Baltimore, MD, 1993.
20. H. Haug and S. W. Koch in *Quantum Theory of the Optical and Electronic Properties of Semiconductors*, (World Scientific, Teaneck, NJ, 1990), chap. 13 and references therein.
21. M. G. Pereira, Jr., S. W. Koch, and W. W. Chow, Appl. Phys. Lett. **59**, 2941 (1991).
22. P. L. Gourley, S. K. Lyo, T. M. Brennan, B. E. Hammons, C. F. Schaus, and S. Sun, Appl. Phys. Lett. **55**,

2698 (1989).
23. P. L. Gourley, T. M. Brennan, B. E. Hammons, S. W. Corzine, R. S. Geels, R. H. Yan, J. W. Scott, and L. A. Coldren, Appl. Phys. Lett. **54**, 1209 (1989).
24. S. W. Corzine, R. S. Geels, J. W. Scott, R. -H. Yan, and L. A. Coldren, IEEE J. Quantum Electron. **25**, 1500 (1989).
25. M. Y. A. Raja, S. R. J. Brueck, M. Osinski, C. F. Schaus, J. G. McInerney, T. M. Brennan, and B. E. Hammons, IEEE J. Quantum Electron. **25**, 1513 (1989).
26. D. Deppe, Appl. Phys. Lett. **57**, 1721 (1990).
27. E. F. Schubert, A. M. Vredenberg, N. E. H. Hunt, Y. H. Wong, P. C. Becker, J. M. Poate, D. C. Jacobson, L. C. Feldman, G. J. Zydzik, Appl. Phys. Lett. **61**, 1381 (1992).
28. G. C. Osbourn, P. L. Gourley, I. J. Fritz, R. M. Biefeld, L. R. Dawson, and T. E. Zipperian, in *Principles and Applications of Semiconductor Strained-Layer Superlattices*, Semiconductors and Semimetals, Vol. 24, chap. 8, edited by R. Dingle, (Academic Press, London, 1987).

29. A. R. Adams, Electron. Lett. **22**, 250 (1986).
30. E. Yablonovitch and E. O. Kane, J. Lightwave Technol. **LT-4**, 504 (1986).
31. D. F. Welch, W. Streifer, C.F. Schaus, S. Sun, and P. L. Gourley, Appl. Phys. Lett. **56**, 10 (1990).
32. P. L. Gourley, S. K. Lyo, and L. R. Dawson, Appl. Phys. Lett. **54**, 1397 (1989).
33. G. Hasnain, J. D. Wynn, S. Gunapala, R. E. Leibenguth, paper JThA2, Quantum Electron. and Laser Sci. Conf. May 10-15, 1992, Anaheim, CA.
34. For a general reference see, G. P. Agarwal and N. K. Dutta, in *Long Wavelength Semiconductor Lasers*, (Van Nostrand-Reinhold, New York, 1986), chap. 6.
35. P. L . Gourley, Appl. Phys. Lett. **57**, 2410 (1990).
36. A. Mukherjee, M. Mahbobzadeh, C. F. Schaus, and S. R. J. Brueck, Photon. Tech. Lett. **2**, 857 (1990).
37. M. B. Sinclair, P. L. Gourley, T. M. Brennan, B. E. Hammons, and L. R. Dawson, Appl. Phys. Lett., submitted.
38. H. R. Karin, L. G. Melcer, R. Nagarajan, J. E. Bowers, S. W. Corzine, P. A. Morton, R. S. Geels, and L. A. Coldren, Appl. Phys. Lett. **57**, 963 (1990).
39. J. M. Wiesenfeld, G. Hasnain, G. C. Damen, J. Shah, J. D. Wynn, R. E. Leibenguth, Y. H. Wang, and A. Y. Cho, paper FW-1, Optical Society of America meeting, Albuquerque, NM, Sept. 20-25, 1992.
40. G. R. Hadley, Opt. Lett. **15**, 1215 (1990).
41. M. Orenstein, E. Kapon, N. G. Stoffel, L. T. Florez, and J. P. Harbison, paper CPDP29-1, Conf. on Lasers and Electro-Optics, May, 1990, Anaheim, CA.
42. H. -J. Yoo, A. Scherer, J. P. Harbison, L. T. Florez, E. G. Paek, B. P. Van der Gaag, A. Von Lehmen, E. Kapon, and Young-Se Kwon, Appl. Phys. Lett. **56**, 1198 (1990).
43. M. E. Warren, P. L. Gourley, G. R. Hadley, G. A. Vawter, T. M. Brennan, B. E. Hammons, and K. L. Lear, Appl. Phys. Lett. **61**, 1484 (1992).
44. P. L. Gourley, M. E. Warren, G. A. Vawter, T. M. Brennan, and B. E. Hammons, Appl. Phys. Lett. **60**, 2714 (1992).
45. C. Kittel, in *Introduction to Solid State Physics*, 4th edition (Wiley, New York, 1971), Advanced Topic A, p. 695.
46. A. Yariv and P. Yeh, in *Optical Waves in Crystals* (Wiley, New York, 1984), chap. 4.
47. P. St. J. Russell, J. Appl. Phys. **59**, 3344 (1986).
48. E. Yablonovitch, Phys. Rev. Lett. **58**, 2059 (1987).
49. K. M. Ho, C. T. Chan, C. M. Soukoulis, Phys. Rev. Lett. **65**, 3152 (1990).
50. R. D. Meade, K. D. Brommer, A. M. Rappe, and J. D. Joannopoulos, Appl. Phys. Lett. **61**, 495 (1992).

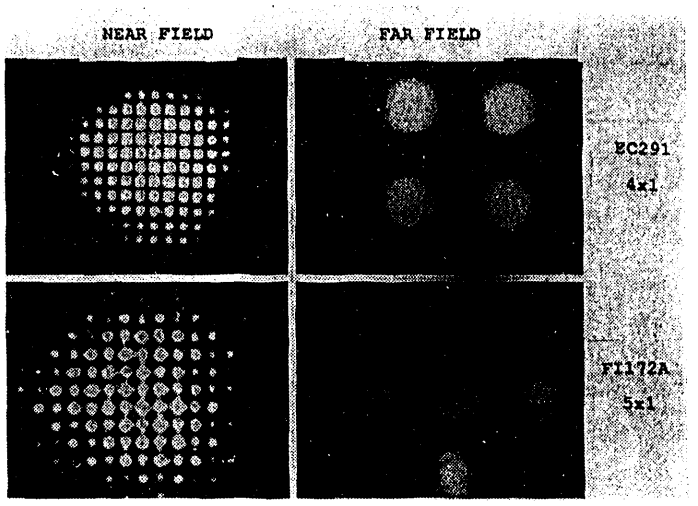

Fig.9
Near and far field patterns for a 2-dimensional array with and without phase compensation by a binary optics phase mask.

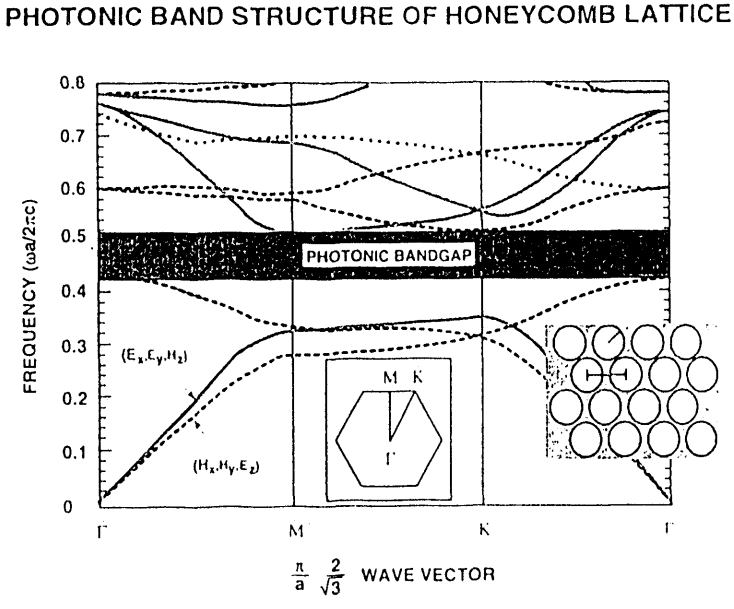

Fig.10
Photonic band structure of a honeycomb nanostructure (triangular lattice of air columns in GaAs) showing complete photonic bandgap. (Figure reproduced from the calculations reference 50 by permission of the authors).

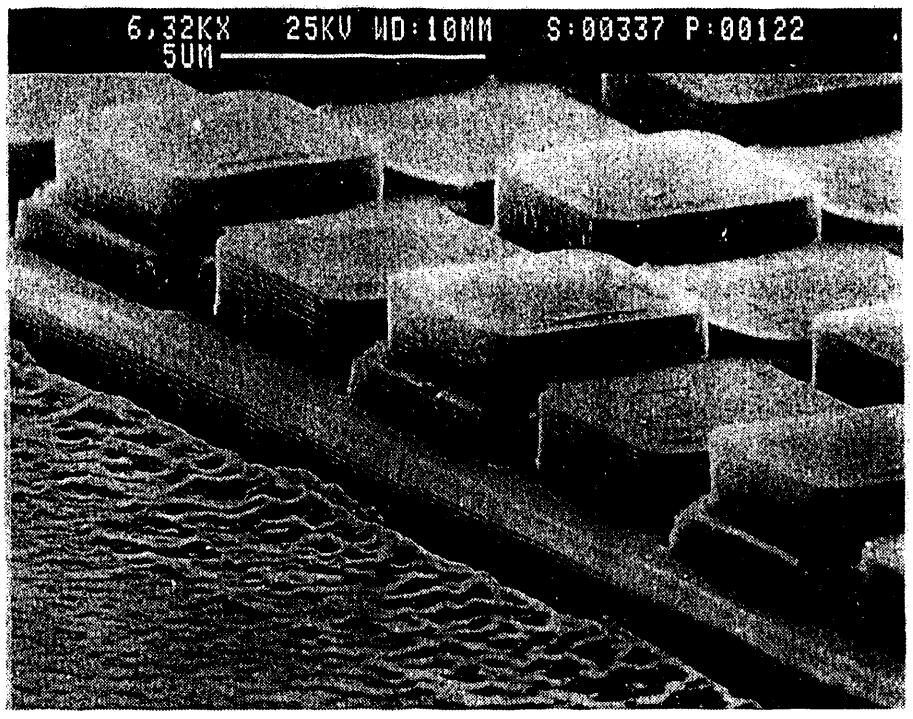

Fig.1
Scanning electron micrograph of a phase-compensated and phase-locked 2-dimensional vertical cavity surface-emitting laser array showing complex microstructure created by layered epitaxy and surface patterning.

Fig.2
Scanning electron micrograph of a vertical cavity surface emitting laser wafer showing layer-by layer microstructure in the laser resonator.

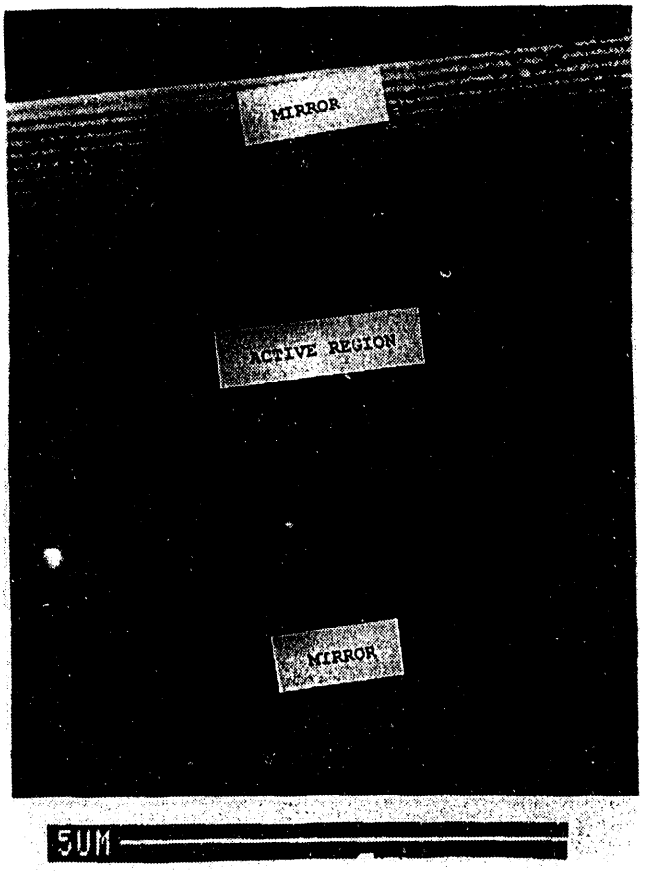

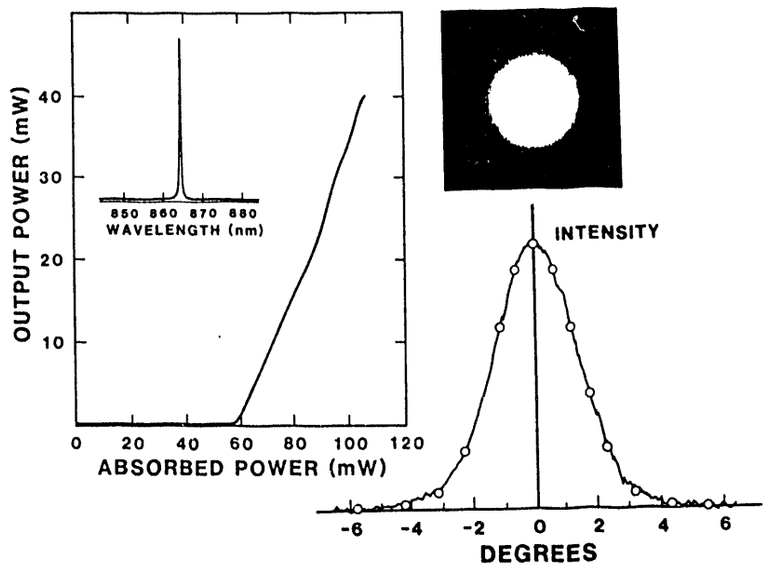

Fig.3
Characteristics of light emitted from a surface-emitting laser wafer, including input-output power curve, lasing spectrum, beam cross section photo, and beam profile.

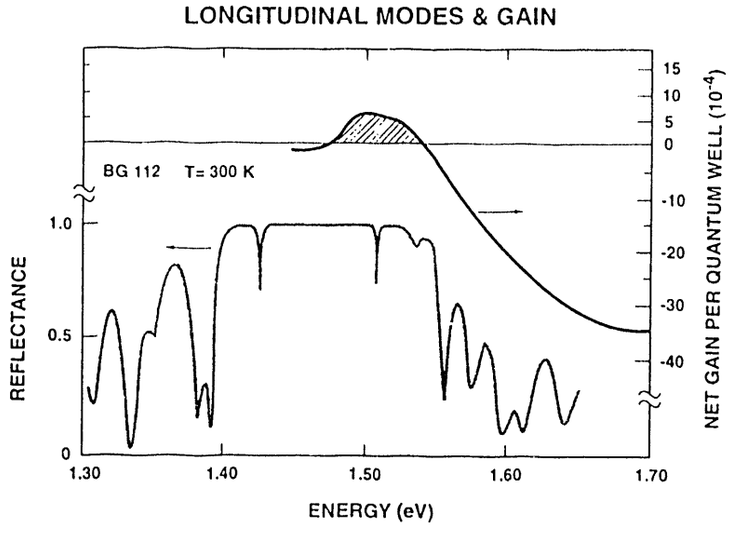

Fig.4
Gain spectrum(upper curve)calculated for a single GaAs/AlGaAs quantum well. Reflectance spectrum (lower curve) of a surface-emitting laser wafer showing high reflectance zone from 1.40 to 1.55 eV and sharp longitudinal optical modes near 1.42 and 1.50 eV.

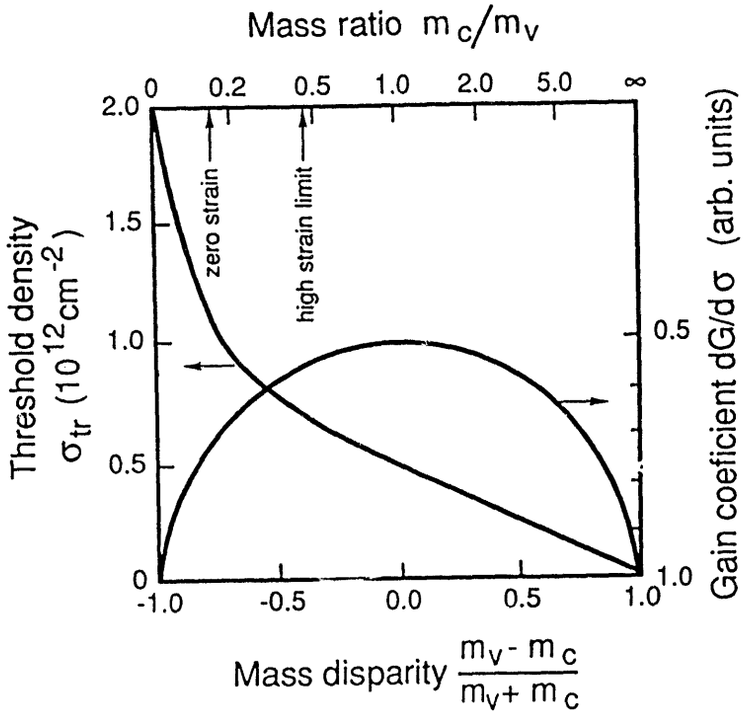

Fig.5
Threshold density (left axis) for lasing and gain coefficient (right axis) as a function of the ratio of the conduction band to valence band masses. The mass ratio for unstrained GaAs and strained-layer InGaAs are indicated by arrows on the upper abscissa.

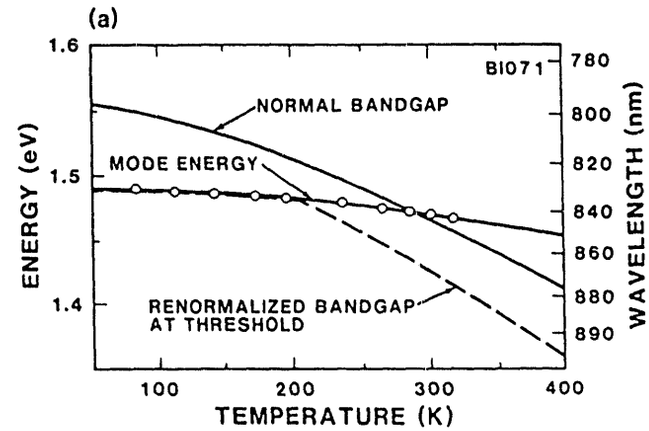

Fig.6
(a) Experimental temperature dependence of the bandgap (solid curve), renormalized bandgap (dashed curve), and lasing mode (open points) energies.

(b) Measured lasing threshold density per quantum well as a function of temperature.

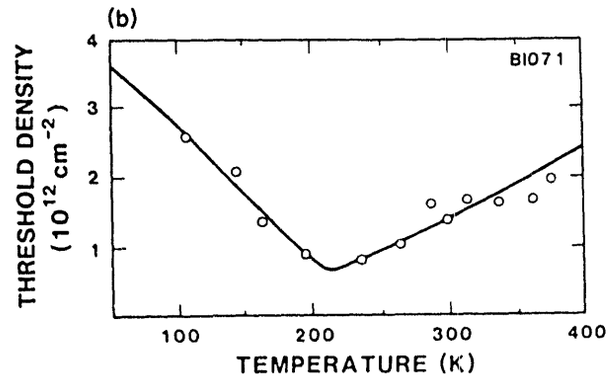

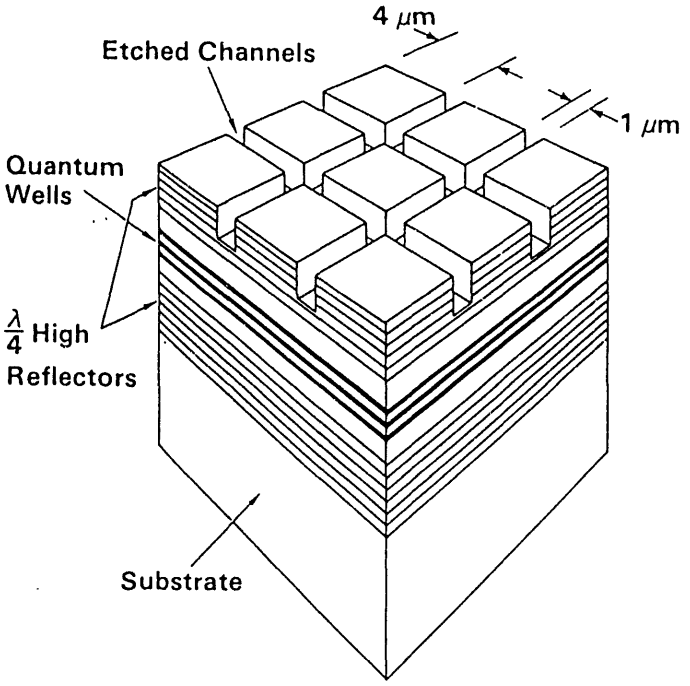

Fig.7
Schematic of a 2-dimensional surface-emitting laser array fabricated by etching channels into the mirror surface.

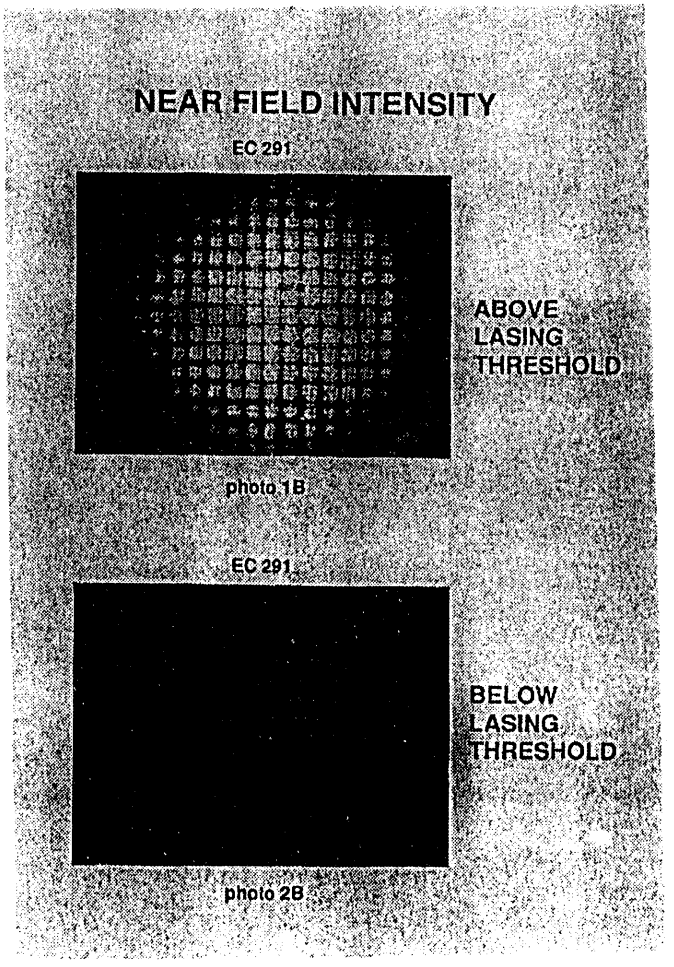

Fig.8
Near field intensity of a photo-pumped 2-dimensional surface-emitting laser array for incident pump power below and above the lasing threshold.

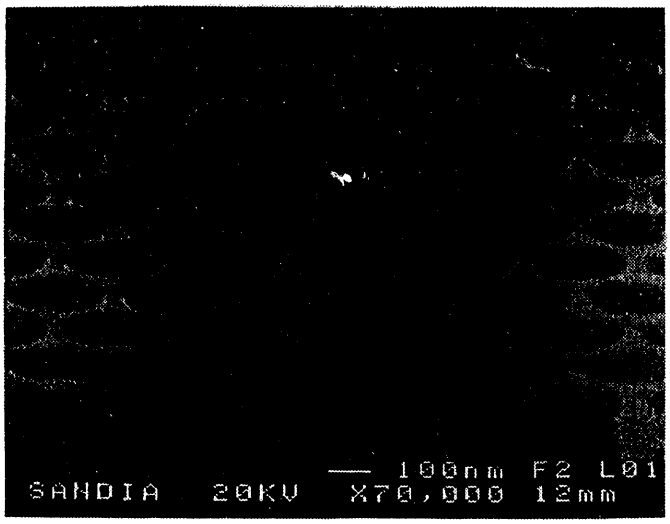

Fig.11
Scanning electron micrograph of a honeycomb nanostructure fabricated in AlGaAs/GaAs materials.

Fig.12
Intensity contour image of 850 nm light (streaks) scattered normally out of the honeycomb plane after propogating through the lattice. The 850 nm is spontaneous emission excited by 750 nm pulses at the boundary of the lattice. The lattice size is 0.8mm square.

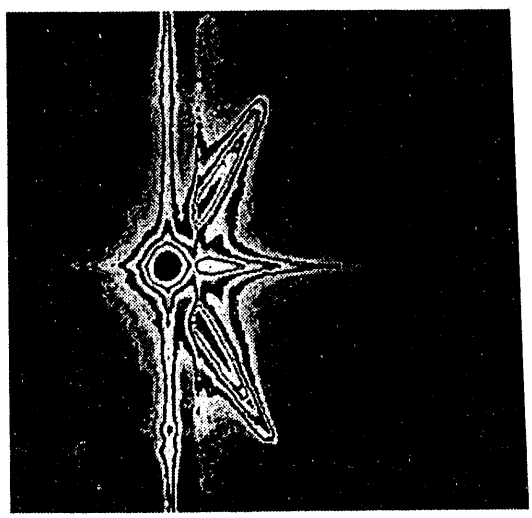

END

DATE
FILMED
3/17/94